

# Journal of Materials Chemistry A

Accepted Manuscript



This is an *Accepted Manuscript*, which has been through the Royal Society of Chemistry peer review process and has been accepted for publication.

*Accepted Manuscripts* are published online shortly after acceptance, before technical editing, formatting and proof reading. Using this free service, authors can make their results available to the community, in citable form, before we publish the edited article. We will replace this *Accepted Manuscript* with the edited and formatted *Advance Article* as soon as it is available.

You can find more information about *Accepted Manuscripts* in the [Information for Authors](#).

Please note that technical editing may introduce minor changes to the text and/or graphics, which may alter content. The journal's standard [Terms & Conditions](#) and the [Ethical guidelines](#) still apply. In no event shall the Royal Society of Chemistry be held responsible for any errors or omissions in this *Accepted Manuscript* or any consequences arising from the use of any information it contains.

## Large-scale controllable preparation and performance of hierarchical nickel microstructures by seed-mediated solution hydrogen reduction route

Junhao Zhang<sup>†, ‡</sup>, Kazumichi Yanagisawa<sup>†,\*</sup>, Shanshan Yao<sup>†</sup>, Hontung Wong<sup>†</sup>, Yushi Qiu<sup>†</sup>,

Hongjuan Zheng<sup>†</sup>

<sup>†</sup>Research Laboratory of Hydrothermal Chemistry, Faculty of Science, Kochi University, 2-5-1 Akebono-cho, Kochi 780-8520, Japan

<sup>‡</sup>School of Environmental and Chemical Engineering; Jiangsu University of Science and Technology; Zhenjiang Jiangsu 212018, China

### Corresponding Author

\*Tel: +81 88 844 8352. Fax: +81 88 844 8362.

Email: [yanagi@kochi-u.ac.jp](mailto:yanagi@kochi-u.ac.jp)

### Notes

The authors declare no competing financial interest.

**ABSTRACT:** As a part of the persistent efforts to accomplish a sustainable society, solution-hydrogen reduction were developed for preparing metal materials. Large-scale hierarchical nickel microstructures with controllable sizes and pores were constructed by adjusting the reaction conditions and the cycles of repeated reduction using nickel nanoparticles about 700 nm as seeds and H<sub>2</sub> as reductant. The investigation results of reaction conditions indicated that ammonia and nickel seeds played crucial roles for the reduction reaction. The possible formation process of self-assembled hierarchical nickel microstructures was proposed based on the results of experiments and analysis. The magnetic hysteresis loops show that the magnetic properties of nickel microstructures were also controllable by controlling the cycles. The hydrogen storage indicates that the hierarchical nickel microstructures have better hydrogen storage performance at 298 K, which may be ascribed reasonably to that H<sub>2</sub> molecules adsorb onto the surface of nickel particles and form activated hydrogen (Ni-H). Such a cost-effective and environmentally friendly procedure is a versatile approach that may be extended to the mass production of some metals and the fabrication of some other hierarchical microstructures.

## 1. INTRODUCTION

Hierarchical micro- and nanostructures of functional inorganic materials have attracted considerable attention due to their highly ordered architectures and well-defined physical properties, which exhibit various potential applications in environmental remediation, optics, and electrochemistry.<sup>1-3</sup> As an important ferromagnetic material, hierarchical nickel particles have attracted much attention both theoretically and experimentally because of their high anisotropy in shapes and structure-dependent magnetic and electronic properties.<sup>4</sup> In past decades, various strategies were used to prepare different hierarchical nickel structures,<sup>5-12</sup> such as hierarchical nickel bowl-like nanostructures by a magnetic self-assembly process,<sup>13</sup> and porous hierarchical nickel nanostructures through a template- and surfactant-free strategy.<sup>14</sup> However, it is still of great importance to explore facile wet-chemical means aiming at simple, economical and environmental benign synthetic approaches independent of surfactants or external magnetic field for assembled nickel hierarchical structures, especially three-dimensional nickel microstructures with mass preparation, controllable size, porosity and density.

Therefore, seeding strategies were devised to fabricate inorganic materials with controlled shape, especially metal materials.<sup>15-18</sup> When small nanoparticles as seeds are added into a solution including metal salt and mild reducing agent, the catalytic reduction of the metal salt on the surface of the metal particles is more readily than that in the bulk solution. This strategy effectively separates the nucleation and growth period of nanoparticle formation. In general, seed-mediated growth of metal particles has several recognized characteristics. It can enhance particle monodispersity relative to the conventional methods, and allow smaller particles to grow into larger particles with a pre-determined size, and take advantage of some properties of seed surface. In the seed-mediated growth, the selection of reducing agent is of great concern, because strong reducing agents can generate new crystal

nuclei in solution, which leads to an undesirable size distribution. Typical reducing agents employed in seed-mediated reduction include sodium borohydride,<sup>19,20</sup> ascorbate ions,<sup>15,16,18</sup> oleyl amine,<sup>21</sup> ethylene glycol,<sup>22,23</sup> glucose,<sup>24</sup> etc. The results also depend on a range of easily controllable parameters, such as reagent concentration, the presence of additives, and the order and rate of addition of reagents. Recently, there is growing interest in green nanotechnology to achieve a sustainable society, which encompasses the use of nanoscale materials for catalysis,<sup>25,26</sup> environmental remediation,<sup>27,28</sup> as well as green methods to reduce or eliminate the use and generation of hazardous substances for the synthesis and production of materials.<sup>29,30</sup> Forsman et al. reported an aerosol phase method to produce cobalt nickel nanoparticles by hydrogen reduction, which is promising for scaling up because of simple process and relatively inexpensive materials.<sup>31</sup>

Toward the goal, solution-hydrogen strategy has been developed to industrially produce metallic nickel and other metals from salt solutions by hydrogen reduction, which is an economical and environmental benign method.<sup>32-38</sup> The works mainly focused on principal phenomena, procedures, catalysts and reaction kinetics. However, few studies were reported about controllable synthesis and structure-dependent properties of metallic nickel and other metals. Here, nickel has been also selected as a model material to investigate the feasibility of the solution hydrogen reduction route for large-scale controllable preparation and structure-dependent properties. In the process, foreign nickel seeds were required to initiate the first reduction; meanwhile, the nickel seeds and obtained nickel could also activate H<sub>2</sub> molecules to form activated hydrogen atoms as reductant. Ammonia was introduced to act as neutralizing agent for controlling pH value and complexing agent for reducing the reaction rate. After the completion of reaction, the depleted solution was discharged, leaving the metallic nickel in the autoclave. The produced nickel particles were used as seeds for the reduction of the next batch of solution. Through repeated batch reductions, the size, porosity

and density could be controlled. However, the repeated batch reductions only continued 10 or 15 cycles because the metal powder particles became too heavy to obtain effective agitation and serve as effective catalysts. This process involves the use of renewable feedstocks, non-hazardous solvent and reductant, and more environmentally responsible reaction conditions.

## 2. EXPERIMENTAL SECTION

### 2.1. Materials.

Nickel (II) sulfate hexhydrate ( $\text{NiSO}_4 \cdot 6\text{H}_2\text{O}$ ), ammonium sulfate ( $(\text{NH}_4)_2\text{SO}_4$ , 98%), and ammonia solution ( $\text{NH}_3 \cdot \text{H}_2\text{O}$ , 28%) were purchased from Wako Pure Chemical Industries, Ltd., Japan. Nickel seeds were obtained from Nissin Rika Co., Ltd. Hydrogen and nitrogen were obtained from Tosa Gas Engineering Co., Ltd. Deionized water was prepared by an Ultrapure Water System (Yamato WG203).

### 2.2. Seed-mediated production of nickel hierarchical microstructures

Preparation of nickel microstructures was carried out in a high pressure autoclave (MMJ-200, OM Lab. Tech. Co., Ltd.) with about  $150 \text{ cm}^3$ . The starting materials including 12.6 g nickel (II) sulfate hexhydrate, 12.4 g ammonium sulfate, 2.8 g nickel seeds about 700 nm (Figure S1(a) of the Supporting Information), 7.7 ml ammonia solution and 18.5 ml deionized water were loaded into the autoclave equipped with a rotor made of Teflon stirring. The temperatures were measured with a K-type thermocouple that was inserted into the autoclave. After sealing the autoclave, the air in the reactor was replaced with  $\text{N}_2$  by successive purging. After the autoclave was heated to  $180 \text{ }^\circ\text{C}$ , 3.5 MPa  $\text{H}_2$  was introduced into the autoclave, and the temperature was maintained at  $180 \text{ }^\circ\text{C}$  for 1 h. Then, the autoclave was cooled to room temperature naturally. It was found that the final products in the autoclave were brown black precipitates and residual gases. The precipitates were collected and washed with distilled water and ethanol for several times. After that, the products were dried in a vacuum box at  $50 \text{ }^\circ\text{C}$  for 6 h, and were collected for characterization. In the repetitive experiments, the obtained

nickel products were used as seeds for the reduction of next batch of the solution. The repeated reduction was conducted up to 10 or 15 times. With increasing repetitive cycles, the color of products becomes to silver gray.

In order to realize mass production, the autoclave with 3 L was used to prepare nickel microstructures, and raw materials were also expanded 20 times under keeping the other reaction conditions unchanged, and the results were consistent with those of micropreparation.

### 2.3 Characterization of nickel hierarchical microstructures

The field-emission scanning electron microscopy (FESEM) images of the seeding agent and products were performed on a JSM-6360 instrument (JEOL). The X-ray powder diffraction (XRD) patterns of the products were recorded on a Rigaku Ultima IV diffractometer operating at 40 kV and 20 mA using Cu K $\alpha$  radiation ( $\lambda=1.54178$  Å). The samples for observing the internal structure were prepared using a cross-section polishing technique with an Ar ion beam (JEOL, SM09010). Low pressure nitrogen (77 K) and hydrogen (77 K and 298 K) adsorption isotherms were performed using an ASAP 2020 instrument (Micromeritics). The distribution of elements was examined by an electron probe micro analysis (EPMA, JXA8900R, JEOL, Japan) under an acceleration voltage of 20 kV, beam current of 10 mA. The average particle sizes were measured by Microtrac 9320HRA, Honeywell, and Autosrb 1-C, Yuasa Ionics. Mercury porosimeter was performed in the pressure range from 0.1 to 60000 psia on a Micromeritics Autopore IV 9500, which mainly shows meso-macropores, total pore volume, total pore area, and the pore size distribution. The nickel production was weighed using electronic balance (HR-200), and the conversion ratio of nickel ions to solid products was define as  $m/m_0$ , where  $m$  and  $m_0$  are the mass of the produced nickel and theoretical mass of complete conversion of the nickel species in starting solution, respectively.

### 3. RESULTS AND DISCUSSION

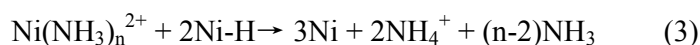
Figure 1a shows the FESEM images of the products obtained from the solution hydrogen reduction route for 1 cycle at 180 °C, which display large-scale uniform hierarchical microstructures about 72  $\mu\text{m}$ , and the yield is almost 100%. The high magnification FESEM images in Figure 1b and 1c show clearly that the microstructures have porous structures formed by assembling smaller particles with the size of about 700 nm. To ascertain the components and structures of products, XRD was used to investigate the crystal phases of the seeds and products obtained for 1 cycle. According to the reflection peaks in the powder XRD pattern in Figure 1d, the main phases of the seeds match well with the face-centered cubic (fcc) structure of nickel (JCPDS 04-850), and the peaks located at 44.5°, 51.8°, and 76.4°, can be indexed to (111), (200), and (220) planes of nickel, respectively. The products obtained for 1 cycle display the same XRD pattern as the seeds, in good agreement with the standard pattern of Ni with fcc structure. No characteristic peaks of other impurities were detected, indicating that pure crystalline nickel microstructures were prepared by the presented procedure.

The slices for observing the internal structures were prepared using a cross-section polishing technique with an Ar ion beam. Figure 2 shows typical cross-sectional FESEM images of a microstructure obtained for 1 cycle. The cross-sectional microstructure in Figure 2a provides definite evidence that nickel hierarchical microstructures are assembled by many small particles and have high porosity. The further observation reveals that the exterior of microstructures is compacter than the interior. Figure 2b shows that the size of small particles is in agreement with the FESEM result in Figure 1c.

Figure 3a shows the nitrogen adsorption-desorption isotherms of the nickel hierarchical microstructures for 1 cycle at 180 °C. The BET surface area is 0.9807  $\text{m}^2/\text{g}$ . The calculation of Barrett-Joyner-Halenda (BJH) in Figure 3b reveals that the pore-size distribution of the

nickel hierarchical microstructures centers between 1.5 and 10 nm. Low pressure hydrogen adsorption measurements of the nickel hierarchical microstructures were carried out at 77 K and 298 K. As shown in Figure 3(c) and 3(d), the results indicate that the nickel hierarchical microstructures has a lower adsorption capacity of 0.00243wt% at 77 K and 860 mmHg, which can be attributed to the big size particles and small BET surface area. It is noteworthy that the value (0.00257wt%) measured for the nickel hierarchical microstructures at 298 K and 860 mmHg is higher than that at 77 K. The result may be ascribed reasonably to that H<sub>2</sub> molecules adsorb onto the surface of nickel particles and form activated hydrogen (Ni-H), which also indicates that the nickel hierarchical microstructures have high activity for hydrogen adsorption at 298 K.

Solution-hydrogen reduction as a simple, economical and environmental benign route was developed to prepare metal materials combined with seed-mediated fabrication. Here, we have selected the important ferromagnetic material, nickel, as a model material for investigation. The overall reaction of nickel reduction was as follows:



In the reaction, the addition of ammonia is done prior to reduction as complexing agent and neutralizing agent. Ammonia with nickel ions forms nickel complexes, shown in equation (1), which can reduce the concentrations of nickel ions in solutions to lower reaction rates, so that the morphology and size of products could be controlled. If no neutralising agent is present, the produced H<sup>+</sup> ions will lower the pH value of the solution, which cause that the reduction is not complete. The results clarify that the amount of ammonia determines the conversion ratios because nickel ions can be reduced by H<sub>2</sub> only when the solution is under

alkaline conditions (Table S1 of the supporting information). Therefore, the amount of ammonia or pH of the solution plays a crucial role in the reduction reaction.

According to our experiments, the self-assembled hierarchical microstructures were difficult to be prepared by the solution-hydrogen reduction without adding seeds, since nickel could not nucleate homogeneously from a solution under the hydrothermal conditions.<sup>39</sup> Nucleation is usually defined as the formation of the smallest thermodynamically stable nucleus of a new phase from parent phase, and solid surface is required to evoke the initial deposition of nickel. So the addition of seeds is important during the initiation of reduction and can also control the rate of the overall reaction. Additionally, it is well known that metallic nickel can be used as hydrogenation catalyst to activate hydrogen.<sup>40,41</sup> H<sub>2</sub> adsorbs on the nickel surface to form Ni-H,<sup>42</sup> shown in equation (2), and the H is in the activated state due to the weak Ni-H bond. The activated hydrogen can release their electrons to Ni<sup>2+</sup> from the dissociation of Ni(NH<sub>3</sub>)<sub>n</sub><sup>2+</sup> in the solution, producing nickel deposited on the surface of nickel seeds, shown in equation (3). Since metallic nickel is the product of reduction, the reaction should become autocatalytic and the reduction reaction is accelerated in the early stages. However, with increasing the cycles, the reduced nickel is deposited on the surface of the nickel already present, causing growth of the solid particles, which means that the effective catalytic area will decrease. Meanwhile, the increase in the density of the growing nickel particles in the course of the reduction makes them settle on the bottom of the autoclave, thereby also decreasing the effective catalytic area. To further investigate the effect of nickel seeds on the controllable preparation of hierarchical microstructures, Figure 4 shows FESEM images of the products obtained by adding 0.8, 1.6, 2.4 g nickel seeds at 180 °C for 1 h and rotation rate of 1200 rpm, which show that the size of microstructures become smaller with increasing the amount of nickel seeds, and the sizes of microstructures are *ca.* 110, 90, 77 μm, respectively. Comparing the high magnification FESEM images in Figure 4c,

4f and 4i, the small particles which are assembled to microstructures, also become smaller and smaller with increasing the amount of nickel seeds. Figure 5 displays the results of grain size analysis of the products obtained by 0.8, 1.2, 1.6, 2.0, 2.4, 2.8 g nickel seeds, which further confirm that the sizes of microstructures decrease with increasing the amount of nickel seeds. Figure 6a indicates that the obtained products mainly comprise two sizes of pores with the average diameters of 1.5 and 33  $\mu\text{m}$ . The results in Figure 6b, 6c and 6d demonstrate that increasing the amount of nickel seeds can improve the total intrusion volume ( $\text{mL/g}$ ) and total pore area ( $\text{m}^2/\text{g}$ ), and lessen the pore sizes of the obtained products. Careful observation from experimental results found that the morphologies of microstructures tend increasingly to spherical shape with reducing the amount of nickel seeds, and the results can be confirmed from FESEM images of the products for 10 cycles using 1.2 g nickel seeds for the first cycle (Figure S2 of the Supporting Information). Another set of experiments was performed to understand the dependence of the morphology and structure of products on nickel seed particle size. From the FESEM images of the products for 1, 5 and 15 cycles using 2.8 g smaller nickel seeds about 200 nm (Figure S1b of the Supporting Information), the morphology and size of the obtained products are not uniform (Figure S3 of the Supporting Information). The reason is that these highly active small particles can accelerate the reduction of  $\text{Ni}^{2+}$  by  $\text{H}_2$ , and lots of nickel atoms are generated in a short time, which cause that it is difficult to fabricate the produced nickel to spherical particles. Therefore, it is very necessary to control the quantity and size of nickel seeds for obtaining the desired products.

Apart from nickel seeds, rotation rate is also one of influence factors in the reduction reaction. The results indicate that conversion ratio was increased with increasing rotation rate before 900 rpm in the reaction of one hour. The variation tendencies of particle sizes and pore information with rotation rate of 750 rpm (Figure S4 and S5 of the Supporting Information)

are similar to the results in Figure 5 and 6. However, in the same other conditions, the sizes of microstructures at 750 rpm are bigger than those at 1200 rpm, and the total intrusion volumes and total pore areas at 750 rpm are slightly higher than those at 1200 rpm. From the FESEM images of the products by adding 0.8, 1.6, 2.4 g nickel seeds at 180 °C for 1 h and rotation rate of 750 rpm (Figure S6 of the Supporting Information), it is also found that the average sizes of microstructures decrease with increasing the amount of nickel seeds, which are *ca.* 166, 139, 98 μm, respectively.

In the reduction reaction, H<sub>2</sub> molecules were activated by nickel catalyst to form Ni-H, and the activated hydrogen acts as reduction reagent to reduce Ni<sup>2+</sup> to Ni<sup>0</sup>, so enough H<sub>2</sub> is very important for complete conversion of nickel ions. When the pressure of H<sub>2</sub> is 3.5 MPa, the nickel ions should be reduced to nickel completely. It is well known that the reduction process from Ni<sup>2+</sup> to Ni<sup>0</sup> needs certain energy, and the reaction temperature would also be an important factor for the reduction reaction. The results of temperature dependence experiments revealed that the reduction reaction has begun at 60 °C, and the nickel conversion ratios were increased until the reaction temperature rose to 80 °C in reduction reaction process of one hour, and Ni<sup>2+</sup> ions in solution have been reduced completely from 80 to 180 °C. The experimental results indicate that the reaction rates were accelerated by higher reaction temperatures, the complete conversion of Ni<sup>2+</sup> needed sixty minutes at 80 °C. However, it was only twenty minutes at 180 °C. This can be rationalized as follows: the decomposition rate of Ni(NH<sub>3</sub>)<sub>n</sub><sup>2+</sup> is accelerated at higher reaction temperature, which will improve the supply of Ni<sup>2+</sup> in solution; higher temperature can also provide high energy for the reduction. Beside the conversion ratio, reaction temperature also influenced the morphology of the products. Figure 7a shows that the products are large scale irregular microstructures with the size of about 30 μm when the reaction temperature is 80 °C, and the microstructures are assembled by many nanoparticles loosely, shown in Figure 7b. With

increasing the reaction temperature, the size and density of microstructures are improved. When the reaction temperature is 120 °C, the products consist of the smaller microstructures with the size of about 30  $\mu\text{m}$  and bigger microstructures in Figure 7c. Figure 7d shows that the sizes of some bigger microstructures reach above 100  $\mu\text{m}$ . From Figure 7e and 7f, when the temperature is increased to 160 °C, the shape of microstructures becomes more uniform, and the size of microstructures is about 75  $\mu\text{m}$ .

The possibility for growing successively to spherical microstructures with controllable size, density and porous structures was investigated by adjusting the cycles of repeated reduction. By repeating the process, the intended target was achieved, and the size, density and porous structure of nickel microstructures could be controlled. Figure 8 shows the FESEM images of the products obtained for 3, 5, 10, 15 cycles. The reduction after 3 cycles still gave uniform hierarchical microstructures with the average size of about 77  $\mu\text{m}$  (Figure 8a). However, the high magnification FESEM images in Figure 8b and 8c show clearly that the porosity become small and the size of small particles become bigger comparing with those of the microstructures obtained for 1 cycle. The results from porosimetry in Figure 9 show that the total intrusion volume, total pore area and average pore size of the microstructures are 0.9561 mL/g, 1.011  $\text{m}^2/\text{g}$  and 3.7839  $\mu\text{m}$  for 1 cycle. When 3 cycles were carried out, the total intrusion volume, total pore area and average pore size are reduced to 0.3842 mL/g, 0.337  $\text{m}^2/\text{g}$  and 4.5534  $\mu\text{m}$ , respectively. Figure 8d, 8e and 8f show the different magnification FESEM images of the products for 5 cycles. The results display that the products are hierarchical microstructures with the average size of about 83  $\mu\text{m}$ . However, there are some small microstructures, which maybe that some small particles were broken off from the incompact structures during mixing process, then growing to the small microstructures in Figure 8d. From Figure 8e and 8f, the porosity of hierarchical microstructures becomes smaller incessantly, and the particle sizes at surface become bigger

obviously. The total intrusion volume, total pore area and average pore size are 0.2119 mL/g, 0.148 m<sup>2</sup>/g and 5.7439 μm, respectively. With increasing the cycles, the sizes of microstructures continue to grow, and the porosity also gradually becomes smaller. From Figure 8g, 8h and 8i, the size of the microstructures for 10 cycles is about 107 μm, and there are almost no pores from the surface of microstructures. The total intrusion volume, total pore area and average pore size are only 0.0993 mL/g, 0.015 m<sup>2</sup>/g and 26.4318 μm, respectively. After 15 cycles, Ni<sup>2+</sup> becomes more and more difficult to completely converse to nickel in the reaction time of one hour. After 15 cycles, the different magnification FESEM images of the products show in Figure 8J, 8k and 8l. The particles become more uniform with the size of about 123 μm, and the surface of microstructures become smooth. The total intrusion volume, total pore area and average pore size are 0.0964 mL/g, 0.010 m<sup>2</sup>/g and 36.8734 μm, respectively. The total intrusion volume and total pore area are reduced constantly, and the average pore size become bigger and bigger with increasing cycles. From Figure 9d, there still exist low peaks centered at about 26 μm, and the peaks centered at about 1.5 μm have disappeared after ten cycles, which indicate that there are no pores or close pore in the interior of the microstructures. The results of XRD in Figure 10 indicate that the products obtained for 3, 5, 10, 15 cycles are also pure crystalline nickel (JCPDS 04-850) and no impurities were detected. When the reactor with 3 L was used to prepare nickel microstructures, and raw materials were also expanded 20 times under keeping the other reaction conditions unchanged, the morphologies and structures of products are similar to those of the products obtained by the reactor with about 150 mL.

Figure 11 shows typical cross-sectional FESEM images of the products obtained for 15 cycles. From Figure 11a, it is difficult to observe obvious pores except several big pores in central section, which indicates that the microstructures become more and more compact with increasing the cycles. However, the high magnification FESEM image in Figure 11b reveals

that there are still some small pores in the inside of microstructures, and these pores should be closed pores combined with the results in Figure 8k and Figure 9, which resulted in that  $\text{Ni}^{2+}$  and  $\text{H}_2$  were retarded to enter the interior of the microparticles. Figure 11c and 11d show EPMA elemental micromaps of Ni and O for nickel slices from the microstructures for 15 cycles. The element distribution on the cross-sections indicates that only Ni element is found on the slices, and the distribution of Ni element is uniform. It is worthwhile to note that neither O element nor other elements were detected. The results match well with the result of XRD analysis.

To elucidate clearly the fabrication mechanism of hierarchical nickel microstructures by seed assisted solution hydrogen reduction route, an illustrative scheme is presented in Figure 12. When  $\text{H}_2$  was added into the reaction solution,  $\text{H}_2$  molecules first adsorbed onto the surface of nickel seeds to form activated hydrogen (Ni-H). The hydrogen with high activity was easy to react with nickel ions in the solution, and the produced nickel deposited on the surface of nickel seeds. Then the produced nickel particles acted as nucleator and hydrogenation catalyst to promote sequentially the reduction reaction between  $\text{Ni}^{2+}$  and  $\text{H}_2$ . In this progress, the reaction became autocatalytic to form hierarchical microstructures until the end of the reaction. In order to control the size and pore of microstructures, some reaction conditions were adjusted, including the amount and size of seeding agent, the amount of ammonia, reaction temperatures, rotation rate, and so on. If need to prepare dense microstructures, the repeating the process by adjusting cycles should be carried out.

It is well known that understanding the relationship between the size, hierarchical surface and magnetic property is very important for fundamental research and the development of potential applications in electronics and information technologies. Magnetic measurements were carried out on the obtained nickel microstructures. Therefore, Figure 13(a) is the magnetic hysteresis loop of as-prepared nickel microstructures for 1, 3, 5, 10 and

15 cycles at 298.15 K. Figure 13(b) displays the relationship between the magnetic properties and cycles. Figure 1 and Figure 7 show a distinct difference in anisotropy, size and hierarchical surface of the microstructures with the increasing of cycles. Since the coercivity of magnetic material depends strongly on size and shape anisotropy. The results indicate that the  $H_c$  values of obtained nickel microstructures are *ca.* 46.7, 16.1, 10.6, 7.1 and 5.4 Oe for 1, 3, 5, 10 and 15 cycles, which decrease with the increase of cycles. Compared with the coercivity value (0.7 Oe) of bulk nickel, obvious increase occurs in the coercivities of all the nickel microstructures, which is consistent with previous reports.<sup>43</sup> The enhancement may be attributed to the reduced size of nickel particles and presence of hierarchical structure which cause change in the magnetization reversal mechanism.<sup>44</sup> The decrease in coercivity of the nickel microstructures with the increase of cycles has been considered to the result from the decrease in the magnetic anisotropy. The values of saturation magnetization ( $M_s$ ) for the as-prepared nickel microstructures decreased from 86.3, 77.1, 69.4, 62.2 to 59.5 emu/g with increasing the cycles, which are bigger than that of the bulk nickel (*ca.* 55 emu/g), possibly for its small sized structures. Additionally, the values of  $M_s$  decrease with increasing the cycles, which is also attributed to the sizes of nickel particles. The same trend was recorded for the remanence magnetization. The results confirm that the coercivity and magnetization are mainly governed by the particle size. Here, shape anisotropy also affects the coercivity and magnetization because of the hierarchical surfaces of the nickel microstructures. This is that the demagnetizing field will not be equal for all directions when particles are not perfectly spherical.

#### 4. CONCLUSIONS

In summary, a seed-mediated growth strategy was developed to fabricate hierarchical nickel microstructures by solution-hydrogen reduction. The results demonstrate that it is possible to control the size, density, and porous structure of nickel microstructures by

adjusting the cycles of the repeated reduction. The synthetic conditions were also investigated and discussed, including the amount and size of nickel seeds, ammonia solution, reaction temperature, reaction time, and so on. The results indicate that nickel seeds and ammonia play key roles in the fabrication of hierarchical nickel microstructures. For example, nickel seeds acted as nucleus to provide control over the nucleation step and evoked the initial deposition of nickel, but also as hydrogenation catalyst to activate H<sub>2</sub>. A possible reaction mechanism was proposed on the basis of the experimental results and analysis. The results of hydrogen storage indicates that the hierarchical nickel microstructures have better hydrogen storage capacity at 298 K than that at 77 K, which was attributed to that the formation of activated hydrogen (Ni-H) on the surface of nickel particles improved the hydrogen adsorption quantity and stability at 298 K. The magnetic properties of nickel microstructures were also controlled, and the coercivities and magnetizations have obvious decrease with increasing the cycles due to the reduced size and presence of hierarchical structure. The nickel microstructures could broaden the application of nickel materials, such as batteries and catalysts as well as stainless steel.

## ACKNOWLEDGMENTS

The work was financially supported by the research fund from Sumitomo Metal Mining Co., Ltd, Natural Science Foundation of Jiangsu Province (No. BK20141293), Natural Science Foundation of the Higher Education Institutions of Jiangsu Province (No. 13KJB430012), the Opening Project of State Key Laboratory of Fire Science (No. HZ2015-KF03), and Qing Lan Project (No. 1614101401).

## REFERENCES

- (1) Xu, L.; Yang, X. Y.; Zhai, Z.; Gu, D. X.; Pang H.; Hou, W. H. *CrystEngComm* **2012**, *14*, 7330-7337.

- (2) Tseng, T. K.; Choi, J. H.; Jung, D. W.; Davidson, M.; Holloway, P. H. *ACS Appl. Mater. Interfaces* **2010**, *2*, 943-946.
- (3) Gutiérrez, M. C.; Hortigüela, M. J.; Amarilla, J. M.; Jiménez, R.; Ferrer, M. L.; del Monte, F. J. *Phys. Chem. C*, **2007**, *111*, 5557-5560.
- (4) Zhou, W.; He, L.; Cheng, R.; Guo, L.; Chen, C. P.; Wang, J. L. *J. Phys. Chem. C* **2009**, *113*, 17355-17358.
- (5) Gao, W.; Shen, S. B.; Cheng, Y. J. *Phys. Chem. C* **2013**, *117*, 9223-9228.
- (6) Shi, Z. W.; Walker, A. V. *Langmuir* **2011**, *27*, 11292-11295.
- (7) Zhang, G. S.; Zhao, L. J. *Dalton Trans.* **2013**, *42*, 3660-3666.
- (8) Ni, X. M.; Zhao, Q. B.; Zhang, D. E.; Zhang, X. J.; Zheng, H. G. *J. Phys. Chem. C* **2007**, *111*, 601-605.
- (9) Cao, F.; Deng, R. P.; Tang, J. K.; Song, S. Y.; Lei, Y. Q.; Zhang, H. J. *CrystEngComm* **2011**, *13*, 223-229.
- (10) Liu, Q.; Liu, H.; Han, M.; Zhu, J.; Liang, Y.; Xu, Z.; Song, Y. *Adv. Mater.* **2005**, *17*, 1995-1999.
- (11) Eagleton, T. S.; Searson, P. C. *Chem. Mater.* **2004**, *16*, 5027-5032.
- (12) Senapati, S.; Srivastava, S. K.; Singh, S. B.; Biswas, K. *Cryst. Growth Des.* **2010**, *10*, 4068-4075.
- (13) Zhou, W.; Lin, L. J.; Zhao, D. Y.; Guo, L. J. *Am. Chem. Soc.* **2011**, *133*, 8389-8391.
- (14) Xiong, J. F.; Shen, H.; Mao, J. X.; Qin, X. T.; Xiao, P.; Wang, X. Z.; Wu, Q.; Hu, Z. J. *Mater. Chem.* **2012**, *22*, 11927-11932.
- (15) Azulai, D.; Cohen, E.; Markovich, G. *Nano Lett.* **2012**, *12*, 5552-5558.
- (16) Jana, N. R.; Gearheart, L.; Murphy, C. J. *Adv. Mater.* **2001**, *13*, 1389-1393.
- (17) Rice, K. P.; Saunders, A. E.; Stoykovich, M. P. *J. Am. Chem. Soc.* **2013**, *135*, 6669-6676.

- (18) DeSantis, C. J.; Sue, A. C.; Bower, M. M.; Skrabalak, S. E. *ACS Nano*, **2012**, *6*, 2617-2628.
- (19) Han, S. H.; Cheon, J. Y.; Joo, S. H.; Lee, J. S. *Mater. Res. Bull.* **2013**, *48*, 2333-2339.
- (20) Chen, L.; Shen, Y. H.; Xie, A. J.; Huang, F. Z.; Zhang, W. Q.; Liu, S. X. *Cryst. Growth & Des.* **2010**, *10*, 2073-2082.
- (21) Somodi, F.; Werner, S.; Peng, Z. M.; Getsoian, A. B.; Mlinar, A. N.; Yeo, B. S.; Bell, A. T. *Langmuir* **2012**, *28*, 3345-3349.
- (22) Xia, X. H.; Zeng, J.; Oetjen, L. K.; Li, Q. G.; Xia, Y. N. *J. Am. Chem. Soc.* **2012**, *134*, 1793-1801.
- (23) Zhang, Q.; Li, W. Y.; Moran, C.; Zeng, J.; Chen, J. Y.; Wen, L. P.; Xia, Y. N. *J. Am. Chem. Soc.* **2010**, *132*, 11372-11378.
- (24) Sun, S. D.; Deng, D. C.; Kong, C. C.; Gao, Y.; Yang, S. C.; Song, X. P.; Ding, B. J.; Yang, Z. M. *CrystEngComm* **2011**, *13*, 5993-5997.
- (25) Sarina, S.; Waclawik, E. R.; Zhu, H. Y. *Green Chem.* **2013**, *15*, 1814-1833.
- (26) Gawande, M. B.; Rathi, A. K.; Nogueira, I. D.; Varma, R. S.; Branco, P. S. *Green Chem.* **2013**, *15*, 1895-1899.
- (27) Chen, L. H.; Reddy, N.; Yang, Y. Q. *Environ. Sci. Technol.* **2013**, *47*, 4505-4511.
- (28) Kemp, K. C.; Seema, H.; Saleh, M.; Le, N. H.; Mahesh, K.; Chandra, V.; Kim, K. S. *Nanoscale* **2013**, *5*, 3149-3171.
- (29) Xia, B. H.; He, F.; Li, L. D. *Langmuir* **2013**, *29*, 4901-4907.
- (30) Wang, Y.; Zhang, P.; Liu, C. F.; Huang, C. Z. *RSC Adv.* **2013**, *3*, 9240-9246.
- (31) Forsman, J.; Tapper, U.; Auvinen, A.; Jokiniemi, J. J. *Nanopart. Res.* **2008**, *10*, 745-759.
- (32) Agrawal, A.; Kumari, S.; Bagchi, D.; Kumar, V.; Pandey, B. D. *Hydrometallurgy* **2006**, *84*, 218-224.

- (33) Agrawal, A.; Bagchi, D.; Kumari, S.; Kumar, V.; Pandey, B. D. *Mater. Lett.* **2008**, *62*, 2880-2882.
- (34) Arita, T.; Hitaka, H.; Minami, K.; Naka, T.; Adschiri, T. *J. Supercrit. Fluid.* **2011**, *57*, 183-189.
- (35) Riu, D. H.; Oh, S. T. *Curr. Appl. Phys.* **2012**, *12*, S188-S191.
- (36) Kobayashi, H.; Yamauchi, M.; Ikeda, R.; Kitagawa, H. *Chem. Commun.* **2009**, *32*, 4806-4808.
- (37) Wajszczuk, R. A.; Charwicz, W. A. *Hydrometallurgy* **1994**, *35*, 99-108.
- (38) Zhang, Y. F.; Lewis, A. E. *Chem. Eng. Sci.* **2006**, *61*, 4120-4125.
- (39) Saarinen, T.; Lindfors, L. E.; Fugleberg, S. *Hydrometallurgy* **1998**, *47*, 309-324.
- (40) Choi, J. S.; Zhang, S. H.; Hill, J. M. *Catal. Sci. Technol.* **2012**, *2*, 179-186.
- (41) Sergeev, A. G.; Webb, J. D.; Hartwig, J. F. *J. Am. Chem. Soc.* **2012**, *134*, 20226-20229.
- (42) Mackiw, V. N.; Kunda, W.; Evans, D.J.T. *Modern Developments in Powder Metallurgy*, Plenum Press, New York, **1966**, pp. 15-49.
- (43) Jia, F. L.; Zhang, L. Z.; Shang, X. Y.; Yang, Y. *Adv. Mater.* **2008**, *20*, 1050-1054.
- (44) Zhang, D. Q.; Li, G. S.; Yu, J. C. *Cryst. Growth & Des.* **2009**, *9*, 2812-2815.

## Figure captions

Figure 1. (a-c) Different magnifications FESEM images of the products for 1 cycle at 180 °C for 1 h; (d) XRD patterns of nickel seeds and the above obtained products.

Figure 2. Different magnifications FESEM image of the cross-section of the nickel microstructure for 1 cycle at 180 °C for 1 h.

Figure 3. (a) Nitrogen adsorption and desorption isotherms of the nickel hierarchical microstructure for 1 cycle at 180 °C for 1 h; (b) Pore size distribution of the nickel hierarchical microstructure; (c) Low pressure hydrogen adsorption isotherms of the nickel hierarchical microstructure at 77 K; (d) Low pressure hydrogen adsorption isotherms of the nickel hierarchical microstructure at 298 K.

Figure 4. Different magnification FESEM images of the products for 1 cycle with the rotation speed of 1200 rpm: (a-c) 0.8 g; (d-f) 1.6 g; (g-i) 2.4 g.

Figure 5. Size attributions of the products using different amount (0.8, 1.2, 1.6, 2.0, 2.4, 2.8 g) of nickel seeds with the rotation speed of 1200 rpm.

Figure 6. Pore information of the products using different amount of nickel seeds (0.8, 1.2, 1.6, 2.0, 2.4, 2.8 g) with the rotation speed of 1200 rpm: (a) differential intrusions curve; (b) total intrusion volume; (c) total pore area; (d) the average pore diameter.

Figure 7. Different magnification FESEM images of obtained nickel microstructures at different temperatures: (a-b) 80 °C; (c-d) 120 °C; (e-f) 160 °C.

Figure 8. Different magnification FESEM images of the products: (a-c) 3 cycles; (d-f) 5 cycles; (g-i) 10 cycles; (j-l) 15 cycles.

Figure 9. Pore information of the products for 1, 3, 5, 10, and 15 cycles from the high pressure mercury porosimetry: (a) total intrusion volumes; (b) total pore areas; (c) average pore diameters; (d) differential intrusions with pore size.

Figure 10. XRD patterns of the products for 3, 5, 10 and 15cycles.

Figure 11 (a) and (b) Different magnification FESEM image of the cross-section of the microstructures obtained for 15 cycles; (c) and (d) EPMA micrographs of the cross-section of the products obtained at for 15 cycles: (c) Ni element; (d) O element.

Figure 12. Schematic illustration of the formation mechanism of nickel microstructures.

Figure 13. (a) Magnetic hysteresis loops of nickel microstructures with different cycles at 298.15 K; (b) Coercivity ( $H_c$ ) and remanence magnetization ( $M_r$ ) of nickel microstructures with different cycles.

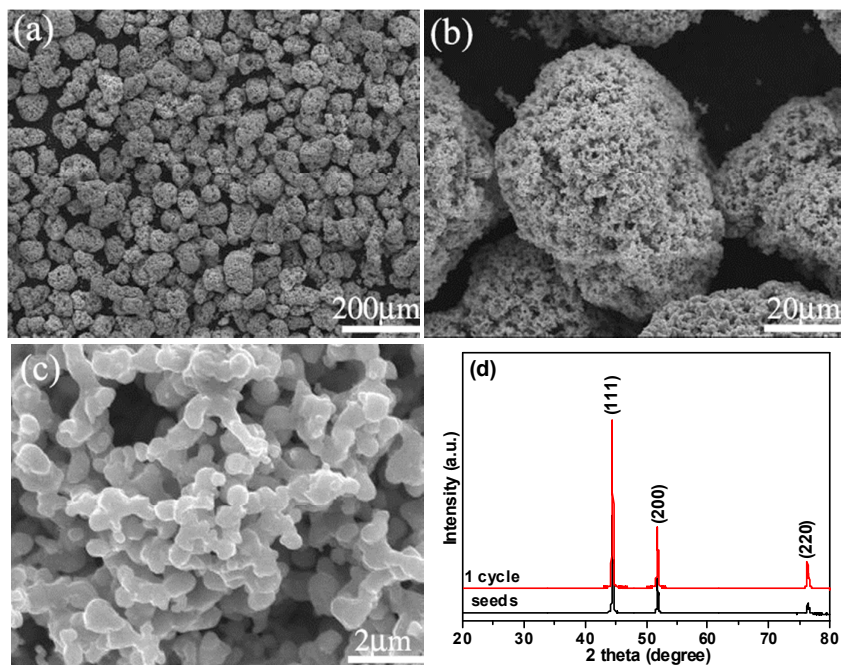


Figure 1

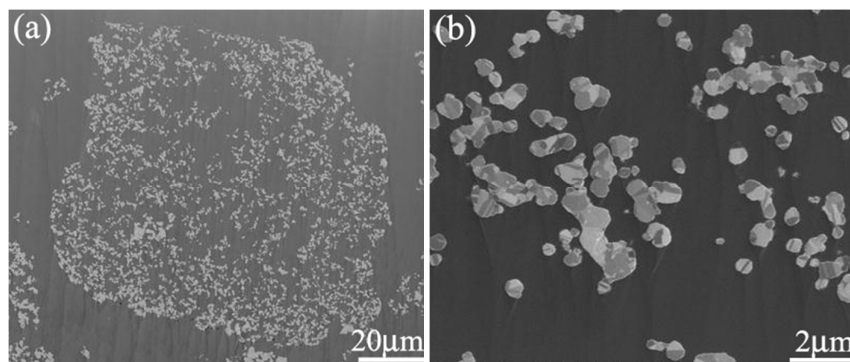


Figure 2

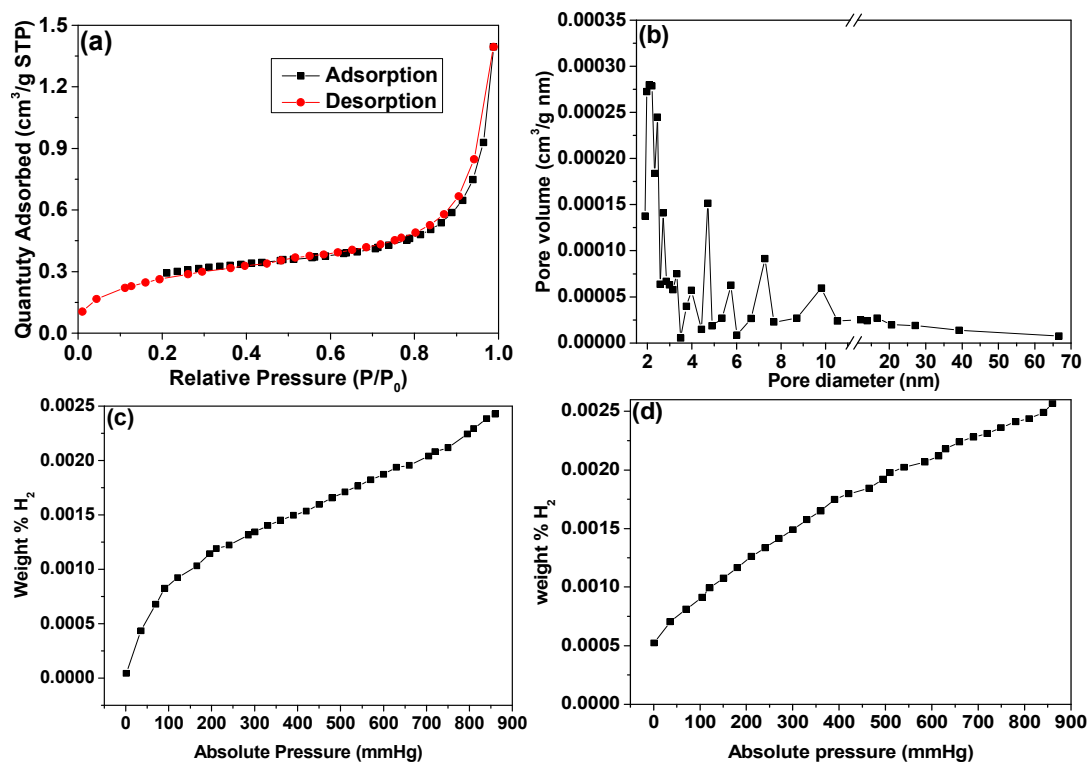
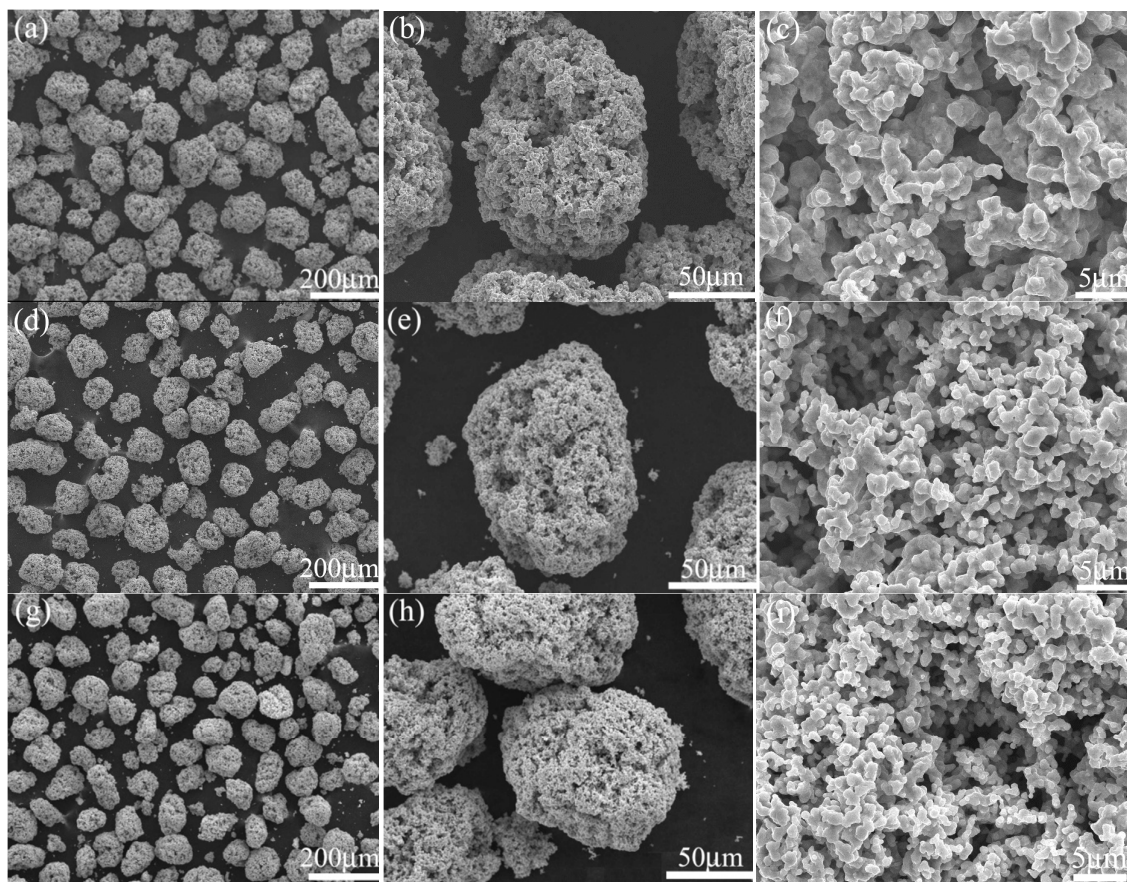


Figure 3

**Figure 4**

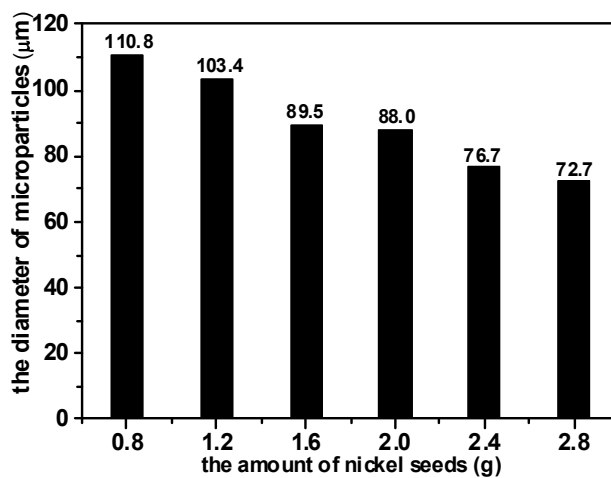
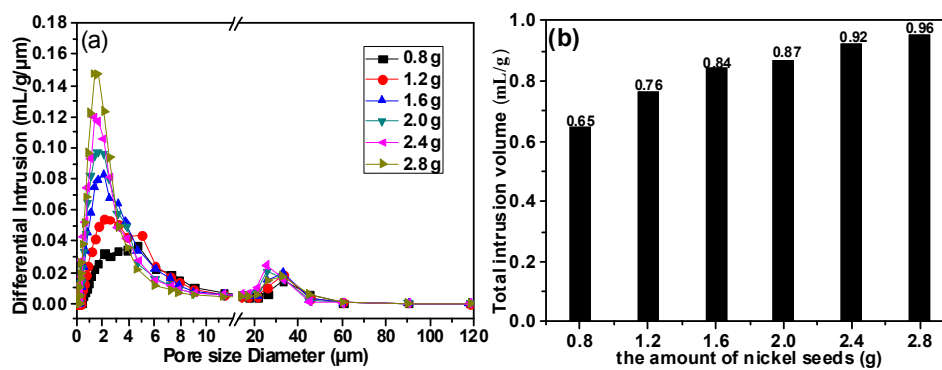


Figure 5



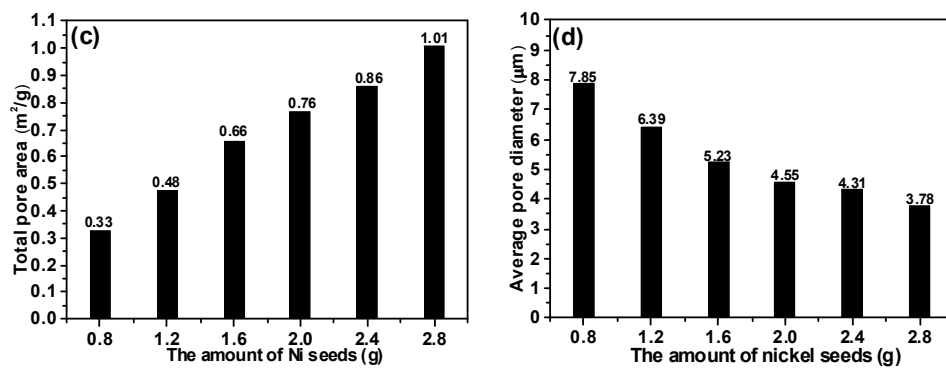
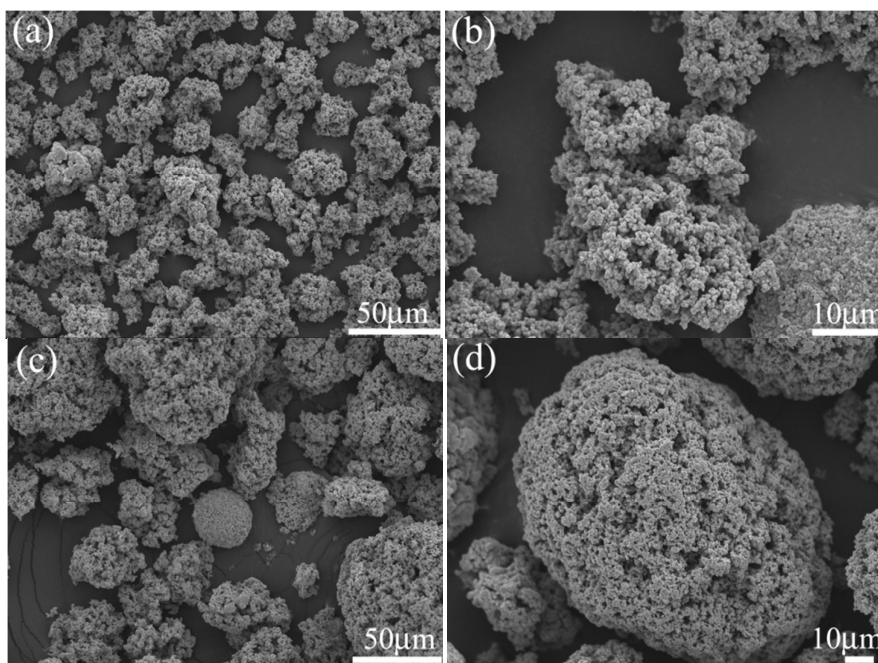


Figure 6



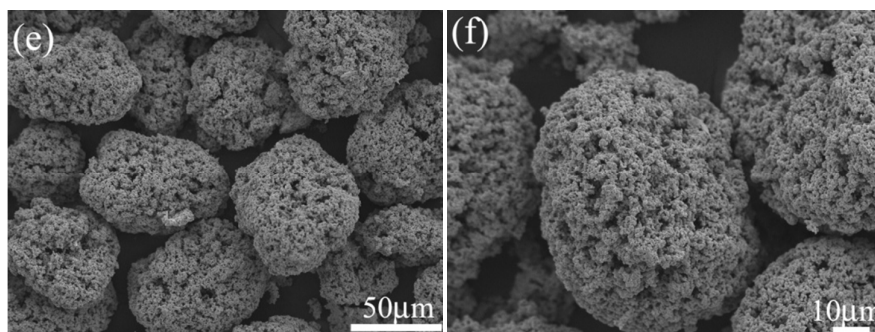
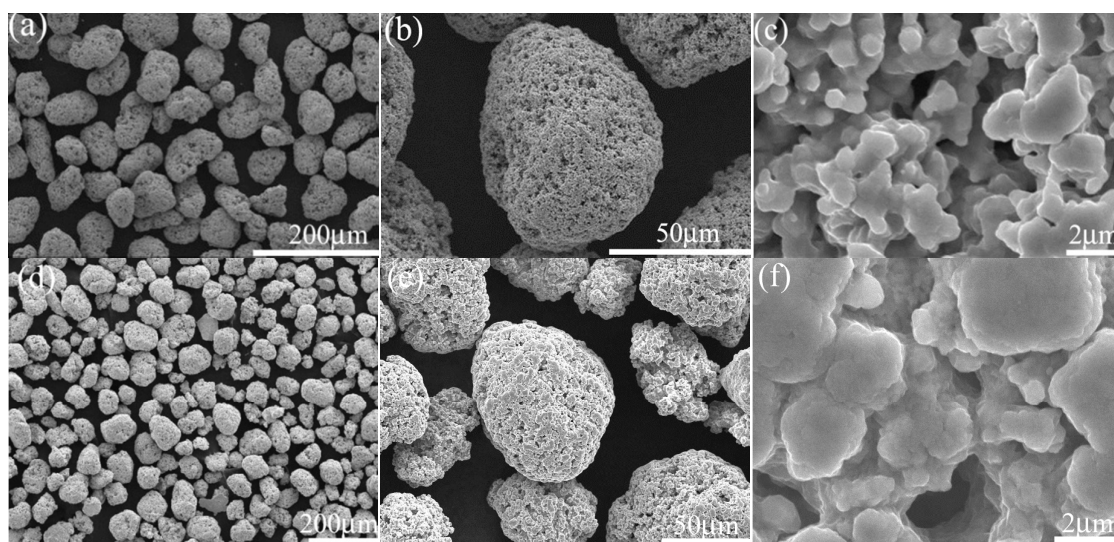


Figure 7



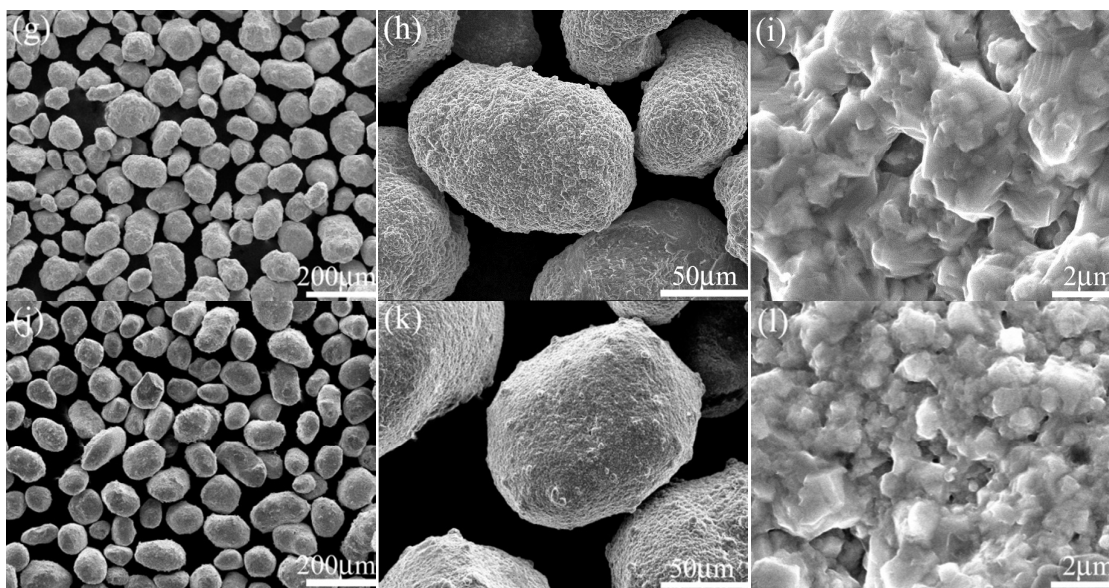
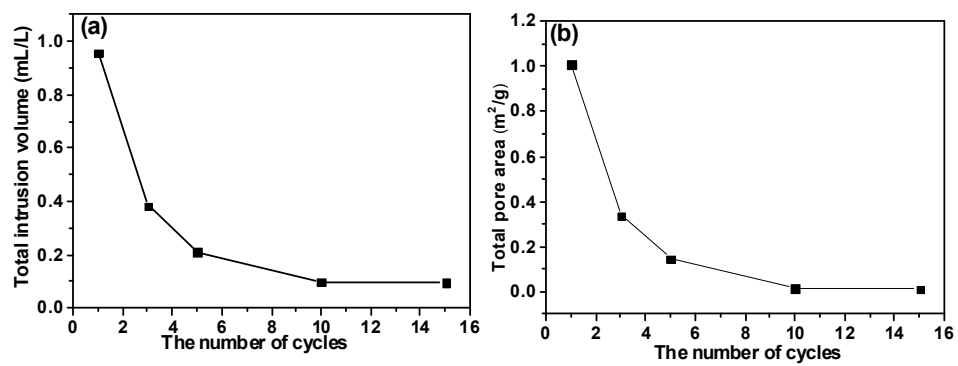


Figure 8



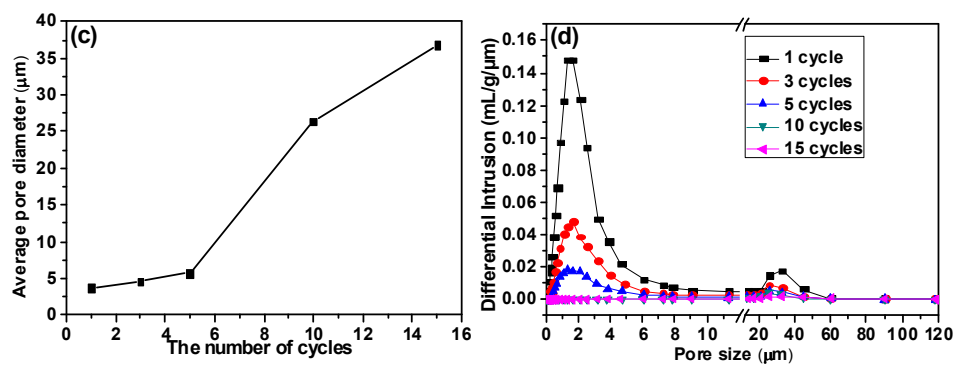


Figure 9

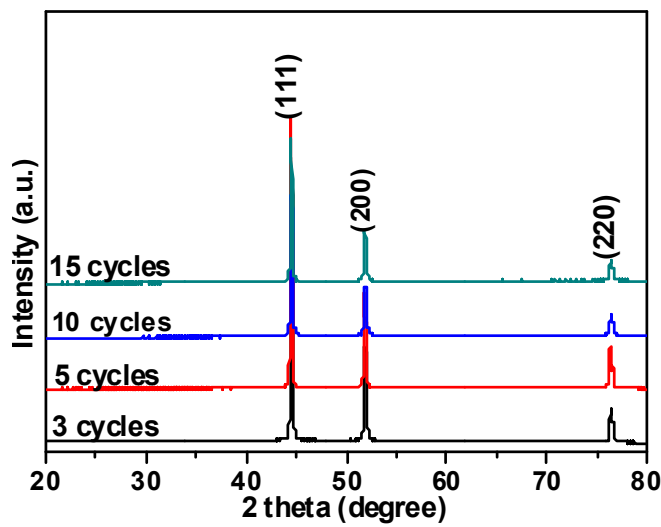


Figure 10

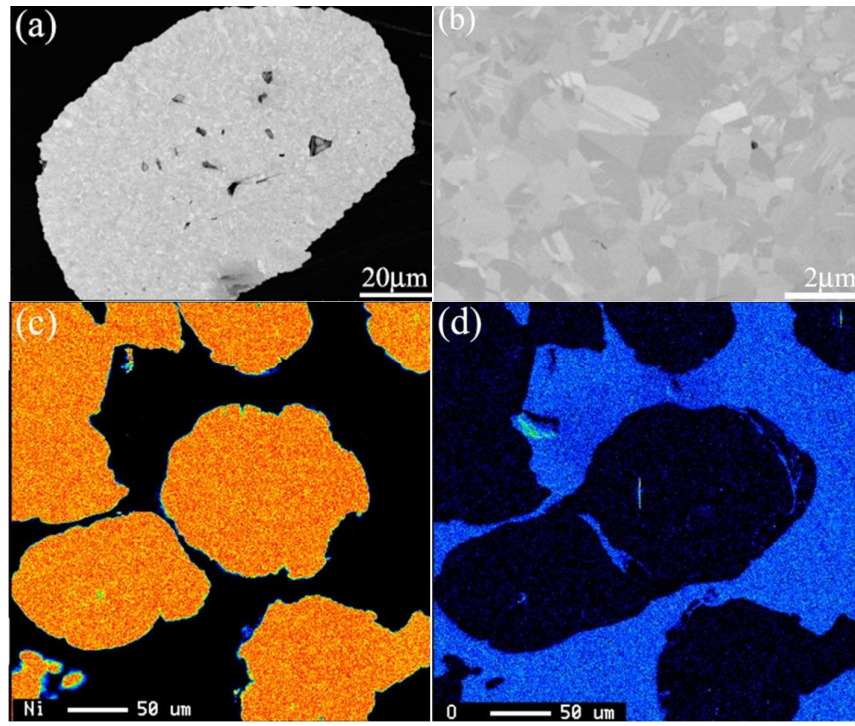


Figure 11

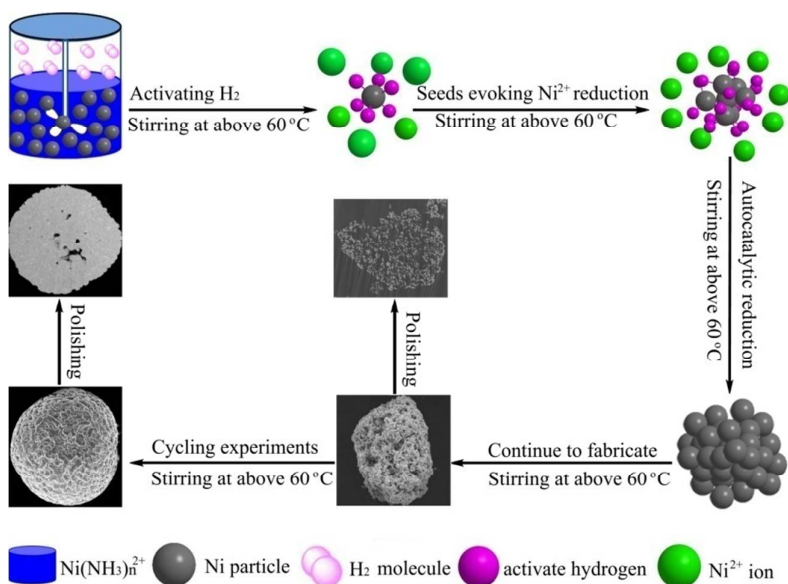


Figure 12

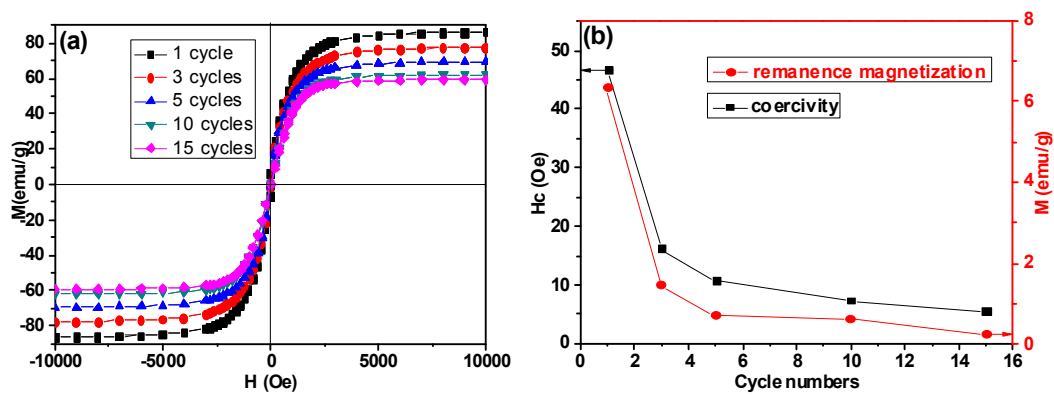


Figure 13